

Part IV

Nanobiomaterials in Biomedical Applications: Diagnosis, Imaging, and Therapy

10

Nonconventional Biosensors Based on Nanomembrane Materials

Lan Yin¹ and Xing Sheng²

¹Tsinghua University, School of Materials Science and Engineering, Beijing 100084, China

²Tsinghua University, Department of Electronic Engineering, Beijing 100084, China

10.1 Introduction

Biosensors have achieved significant progress in the past decades and are now widely used for diagnostic and therapeutic purposes. A biosensor is defined as a device for analyte detection or physiological signal measurements, which usually combines selective biological elements and transducers that convert signals resulting from the interaction between the analyte and biological elements to other easily measured outputs (e.g., electrical, optical, and thermal signals) [1]. A broad range of biomaterials have been involved in building various biosensors. The major components usually include a probe that selectively responds to a certain biological element, such as deoxyribonucleic acid (DNA), aptamer, antibody, enzyme, cell, and so on, and a transducer that transforms the physiochemical information into optical, electrical, magnetic, electrochemical, and thermal signals. Due to the advantages of high surface area, miniaturized size, and associated new physical properties, nanomaterials have drawn a great deal of attention as components for biosensors. The explored nanomaterials can be categorized on the basis of different dimensions, including (i) zero-dimensional (0D) nanomaterials, such as nanoparticles (NPs) and quantum dots (QDs) that have surface plasmon resonance or size-dependent properties; (ii) 1-dimensional (1D) nanomaterials, such as nanowires and nanotubes that offer unique longitudinal electron transport properties and sensitive modulation for field-effect transistor (FET) sensors; (iii) 2-dimensional (2D) nanomaterials, such as nanomembranes and 2D single-layer materials (e.g., graphene or graphene oxides); and (iv) 3-dimensional (3D) nanomaterials, such as 3D assembly of nanomaterials or porous nanostructures that possess interesting properties (e.g., photonic crystals). Based on these nanomaterials, a variety of biosensors have been proposed over the past years, including optical biosensors based on fluorescence spectroscopy and surface-enhanced Raman spectroscopy (SERS), electrical biosensors based on electrochemical or FET biosensing techniques, magnetic biosensors for cancer treatment, and so on. Specific representative biosensors are glucose monitors using amperometric sensing through glucose oxidase, photonic crystal label-free

biosensors by means of a periodic optical nanostructure, neural sensors through measuring electroencephalography (EEG) or electrocorticography (ECoG), and so on. There have been many comprehensive reviews of various biosensors based on a wide range of nanomaterials, different means of immobilization of biological recognition materials, and fabrication techniques based on microfluidic channels and lab-on-chip technologies, as can be found in [1, 2], and so on. Instead of covering the broad spectrum of nanomaterials for biosensors, the scope of this chapter is focused on recent advances of nonconventional flexible, stretchable, and degradable biomedical sensors based on nanomembrane materials.

Traditional electronics for biomedical applications are usually designed to be rigid and planar with a long lifespan, such as the Utah Intracortical Electrode Arrays based on rigid silicon (Si) materials and glucose monitors in the bulk format [3, 4]. When integrating the rigid bioelectronics with the human body to achieve an intimate interface for continuous sensing, the mechanical mismatch at the interface remains as the biggest challenge, since the human body is soft and curvilinear. Recent developments in new materials, manufacturing technology, and design strategies have enabled advances in flexible, stretchable, injectable, and biodegradable biosensors that possess unique capabilities of diagnostic and therapeutic functions [5]. Materials in a nanomembrane format and arranged in a unique configuration have greatly improved the contact properties and therefore enable better integration of biosensors onto or into the human body. Three categories of such nonconventional biosensors are introduced in details, including soft, injectable, and biodegradable electronics.

10.2 Soft Electronics

While most soft electronics are based on organic materials, configuring inorganic hard materials in nanomembrane formats or/and integrating them with soft materials provides a path to build multifunctional sensors with high performance as well as flexible and stretchable characteristics that enable conformal contact with the human body.

Inorganic semiconductor materials are known to be extremely brittle, for example, silicon (Si) breaks when stretched by less than 1% of strain. In order to overcome the intrinsic problem, nanomembranes with small thickness are desirable because the flexural rigidity is significantly reduced as thickness decreases (e.g., the rigidity of 10-nm Si nanomembrane is 12 orders of magnitude smaller compared to that of 200- μm Si) [6]. Therefore, hard semiconductor materials such as Si nanomembranes less than a few hundreds of nanometers become flexible and can accommodate large curvature [7], and can be combined with polymeric substrates to achieve flexible bio-integrated electronics. The development of novel fabrication techniques allows transfer printing of semiconductor nanomembranes or metallic interconnects with excellent operational properties onto flexible substrates. For example, high-quality single-crystal silicon nanomembranes can be obtained from a silicon-on-insulator (SOI) wafer through a transfer printing process, as shown in Figure 10.1a [8]. Transfer printing begins from a soft elastomeric stamp such as (poly)dimethylsiloxane (PDMS),

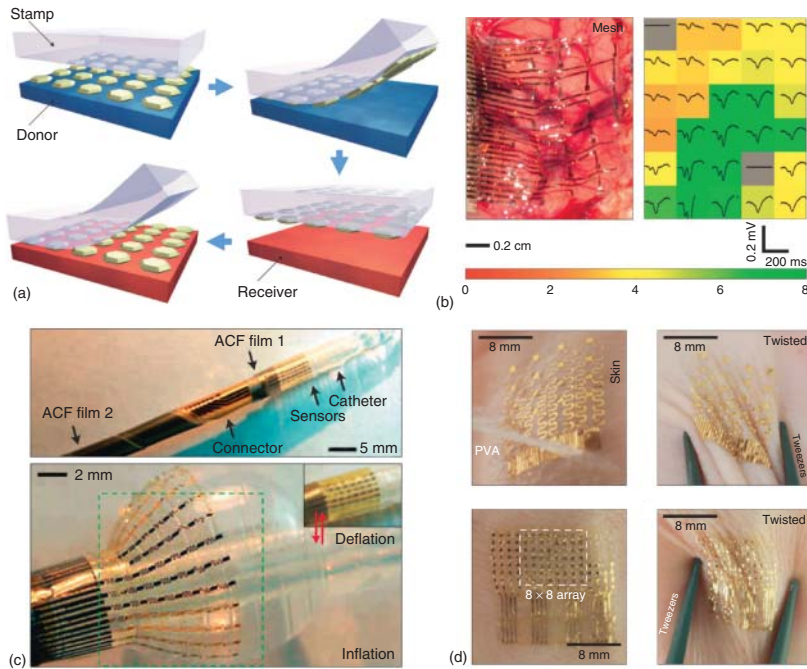


Figure 10.1 *Soft electronics.* (a) Schematic illustration of the transfer printing process. Membrane materials on a donor substrate are released by etching the intermediate sacrificial layer (certain points of the membranes are anchored on the substrate to prevent drifting during the etching process if necessary). A stamp is laminated on the donor substrate to pick up the membranes via a quick motion. To retrieve the nanomembranes, the stamp is pressed against a receiver substrate. By slowly peeling the stamp away, nanomembranes can be released on the target substrates (adhesive layer is applied on the receiver substrate if necessary). (b) (left) Image of the neural electrode array with $2.5\ \mu\text{m}$ PI mesh-type substrate on a feline brain, showing excellent conformal contact. (right) The average evoked response from each electrode in the 200 ms window (the color shows the ratio of the rms amplitude indicating the signal quality, with green suggesting high quality, and red being poor). (c) (top) The overall structure of a deflated catheter integrated with a flexible and stretchable electronic system, including the sensors, connectors, and anisotropic conductive film (ACF) cables. (bottom) Optical image of the inflated balloon catheter with approximate 130% strains compared to its deflated state. (d) Ultrathin epidermal temperature sensor. (top left) 4×4 temperature coefficient of resistance (TCR) sensor array applied to the skin using PVA tape. (top right) Pinching of the skin to induce twisting deformation to the device. (bottom left) 8×8 sensor array with Si nanomembranes mounted on the skin. (bottom right) Same twisting deformation of the device. (With permission from Meitl *et al.* 2006 [8], Nature Publishing Group.) (With permission from Kim *et al.* 2010 [9], Nature Publishing Group.) (With permission from Kim *et al.* 2011 [10], Nature Publishing Group.) (With permission from Webb *et al.* 2013 [11], Nature Publishing Group.)

to pick up nanomembranes released from a source wafer (the donor, e.g., SOI wafer), but is anchored at certain points to avoid drifting of nanomembranes through etching the intermediate sacrificial layer. The pickup action is achieved through adhesion force to PDMS dominated by van der Waals forces, which is rate sensitive. Retrieval of nanomembranes to target substrates (the receiver)

involves strategies to switch in adhesion force, including rate-dependent viscoelastic effects, interfacial bonding layer, and so on. Transfer printing can either be performed over a large area using flat PDMS or over a specific area using specially structured PDMS. Such techniques were successfully demonstrated with materials such as silicon, gallium arsenide (GaAs), indium gallium nitride (InGaN), and so on [8]. In some scenarios, extreme larger bending or stretching could occur when interfacing with the human body, for example, electronics integrated with the skin can reach strain more than 30%, sensors on inflated balloon catheters can undergo deformation even over 100% [7]. One strategy to further accommodate large deformation in bio-integrated electronics is to utilize buckling mechanics [12]. For example, electronics with open mesh layouts is transfer printed onto a prestretched elastomeric substrate with regions of semiconductor islands selectively bonded to the elastomer [7]. Upon releasing of the substrate, interconnects with more flexibility compared to that of the semiconductors delaminate to adopt an arc-shape buckling structure resulting from the compressive stress. When subjected to deformation, interconnects can move freely with changes in amplitude and wavelength. By utilizing such a strategy, the semiconductor materials experience negligible strain and the interconnects undergo reducing strains by orders of magnitude less than those in the elastomer substrate; thus, electronics can deal with extremely large deformation without fracturing. Further improvements are possible involving designs of serpentine or fractal interconnects with similar overall structure [13, 14]. The mechanical design with ultrathin nanomembrane and buckling structure and development of transfer printing techniques greatly broaden the materials' choice of key components with exceptional performance for soft electronics. Combining semiconductor nanomembranes with thin-film interconnects, dielectric materials, and soft polymeric substrates, a variety of flexible and stretchable functional devices were proved to be possible.

Large area arrays of FET and silicon metal oxide semiconductor field-effect transistors (MOSFETs), one of the most important building blocks for electronic devices, were achieved on flexible and stretchable substrates [15–18]. Arrays of silicon solar cells were created from bulk wafers and transferred onto flexible substrates offering high efficiency, great mechanical flexibility, and desirable transparency [19]. Hemispherical electronic eye and arthropod eye camera based on single-crystal silicon nanomembranes were built through transfer printing of circuits fabricated on planar wafers followed by deformation into a curvilinear hemispherical shape, which opens the route to create optoelectronics with unusual geometry from planar microfabrication techniques [20, 21]. Inorganic light-emitting diodes (ILEDs) using epitaxial semiconductor (e.g., GaAs, aluminum gallium indium phosphide (AlInGaP)) thin films can be transferred onto arbitrary substrates with designed spatial distribution, yielding high flexibility that can accommodate large deformation and possess semitransparent characteristics [22, 23]. Based on large area arrays of electronic building blocks, such as FETs, MOSFETs, light-emitting diodes (LEDs), and so on, various biosensors integrating inorganic hard materials and soft polymeric substrates that can intimately wrap around major organs such as the brain, heart, and epidermis have become possible. Neural electrode arrays based on ultrathin

silicon nanomembranes with high density, high temporal resolution, and high-speed multiplexing were achieved to monitor ECoG such as sleep spindles and electrographic seizures [9], as shown in Figure 10.1b. Ultrathin substrates (less than 10 μm) and open mesh geometries enable conformal contact to the brain tissues including the hemispherical fissure area of the brain (Figure 10.1b). Small spacing between the neural electrodes allows observation of microseizure and provides insights into new neural mechanisms. As shown in Figure 10.1b, conformal wrapping of an ultrathin neural sensor on the brain tissue yields excellent recording signals of high root-mean-square (rms) amplitude ratio of 5.7 ± 3.0 . Sacrificial silk substrates were utilized to mount such systems with ultralow bending stiffness on to the brain, which will otherwise be difficult to handle. Upon delivering the biosensor on the brain tissue, dissolution of silk allows conformal coverage and minimal stress at the device and tissue interface, which offers new strategies to ensure intimate brain–machine interface (BMI) that is required for high-resolution and chronic implanted medical devices [9, 24]. Stretchable biosensors can also be fabricated on balloon catheters for large area mapping of temperature and electrogram data, enabling quick assessment of cardiac ablation instead of the conventional point-to-point manual fashion [10]. Carefully designed serpentine interconnects bridge active and passive devices at the nodes of the mesh structure (Figure 10.1c), to minimize the mechanical coupling of the strains and enable large deformations associated with inflation and deflation. The devices show little performance degradation after multiple inflation and deflation cycles, with strains exceeding 100%. Epicardial biosensors with high-density electrodes and multiplexing circuitry based on silicon nanomembranes were also proved to be possible for measurements of both high spatial and temporal resolution [25]. Contact sensors and stimulation electrodes can also be added to the system, allowing guidance of deployment of the platform and can achieve stimulation therapy. Further development of 3D multifunctional integumentary biosensors across the entire epicardium for cardiac measurements, including pH, temperature and mechanical strain, and electrical, thermal, and optical stimulation, have also been achieved [26]. One of the most mature soft electronics based on nanomembranes is the biosensor with ultrathin thicknesses that achieves elastic modulus and bending stiffness comparable to the skin epidermis, and therefore allows the development of “tattoo”-like mechanically imperceptible epidermal device systems [14]. An example of such a device is illustrated in Figure 10.1d [11]. The ultrathin device can be transferred to the skin through a water-soluble tape based on poly(vinyl alcohol) (PVA) with both passive interconnects and active Si nanomembranes. The platform can achieve conformal attachment to the skin through van der Waals forces and can withstand various deformations such as twisting, stretching, or wrinkling on the skin without device delamination or performance degradation. Demonstrated functional systems include hydration and sweat sensors for skincare monitoring [27–29]; fingertip tactile sensors for “instrumented” surgical gloves [30]; skin machine-human sensors for surface electromyography (sEMG) measurements for remote controlling [31]; epidermal thermometers for monitoring blood perfusion, localization of thermogenesis, and vascular reactivity [11]; skin-like biosensors for chronic cutaneous wound healing monitoring [32]; lead

zirconate titanate (PZT) thin-film-based skin sensors for pulse pressure and skin mechanical property measurements [33, 34]; electroencephalogram (EEG) sensors on the auricle as a persistent brain–computer interface [35]; and epidermal wireless systems that allow power transfer and near-field data acquisition [34, 36].

10.3 Injectable Electronics

Delivery of biosensors further into the tissues or organs instead of on the surface can provide more detailed information. Based on the previous mentioned technology, nanomembrane-based injectable biosensors were fabricated on flexible substrates and can be delivered to targeted locations in a minimal invasive fashion through a releasable needle. Integration of micro-inorganic light-emitting diodes (μ -ILEDs), micro-inorganic photo detectors (μ -IPDs), temperature sensors, and stimulating electrodes together with wireless circuitry enables advanced optoelectronic systems to study single-neuron activity associated with complex behavior through the mechanism of optogenetics by activation of light-sensitive proteins [37, 38]. The representative probe is shown in Figure 10.2a [38], with the blue μ -ILED being powered. The detailed structure of the probe is illustrated in Figure 10.2b [38], with the first layer of platinum microelectrodes ($20\ \mu\text{m} \times 20\ \mu\text{m}$ exposed area) for recording and stimulating, the second layer of Si μ -IPD ($1.25\text{-}\mu\text{m}$ thick, $200 \times 200\ \mu\text{m}^2$), the third layer of 4 μ -ILED connected in parallel, and the fourth layer of micro Pt temperature sensors or heaters. Each layer is precisely aligned and stacked to each other with a thin epoxy layer (500 nm), and the whole device is bonded to an epoxy micro-needle using a water-soluble silk layer, which allows the removal of the micro-needle after implantation. *In vivo* flexible optofluidic neural probes combining optogenetics, microfluidics, and pharmacology were also developed, which allows both photostimulation and programmed spatiotemporal drug delivery for deep brain manipulation. The associated wireless system permits remote control in freely moving animals [40]. Similar ideas have been expanded into peripheral nerves and spinal epidural space using flexible systems with commercial chips assembled on metallic nanomembrane circuits encapsulated with elastomer substrates. The system is shown in Figure 10.2c [39]. Major components include commercial radio frequency (RF) harvester, LEDs, and antenna. These units are connected with serpentine metal nanomembrane interconnects (Ti/Au) and the whole circuit is encapsulated by polyimide inside a silicone elastomer, enabling a soft optoelectronic system. Such a device is subdermally implanted to stimulate the peripheral nerve or placed in the epidural space to control the spinal cord, as shown in Figure 10.2d. Through *in vivo* sciatic stimulation, nocifensive responses of genetically modified mice can be manipulated. For example, Advillin-ChR2 and TrpV1-ChR2 mice with sciatic stimulation show clear aversion to LED-on zone, as shown in Figure 10.2e [39]. This research demonstrates that optogenetic biosensors can be well adapted to other organs besides the brain for clinical trials such as chronic pain management [39]. Injectable biosensor platforms capable of temperature measurements were also realized to assess thermal conductivity and heat capacity for cardiac

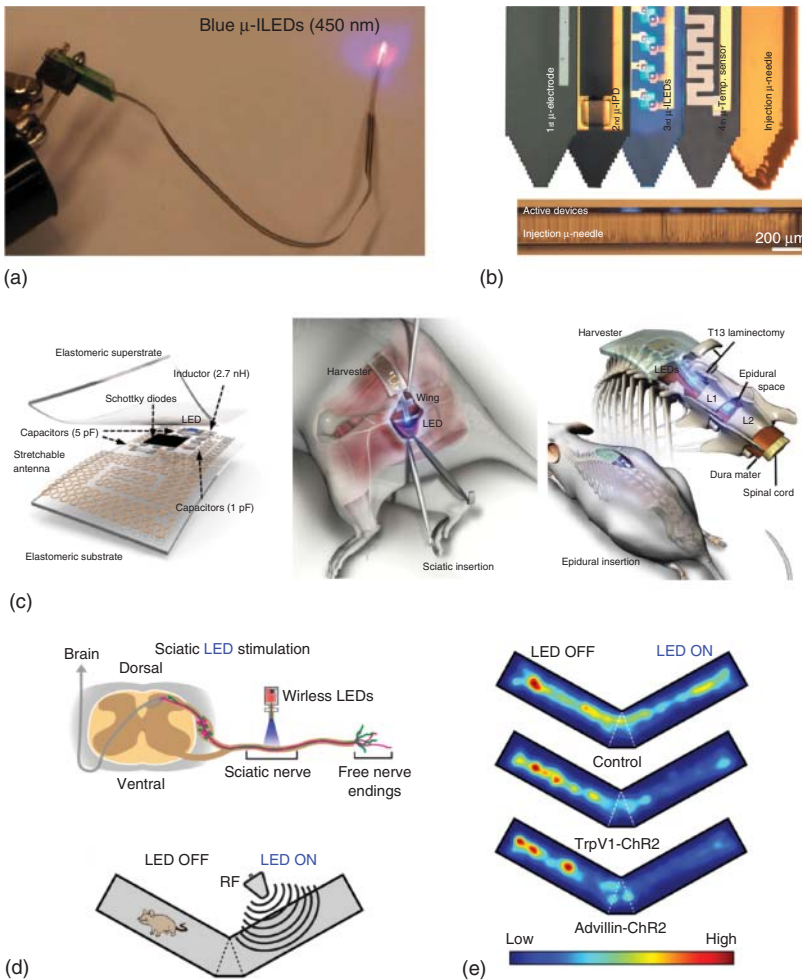


Figure 10.2 *Injectable electronics.* (a) Injectable micro-needle integrated with electronics with the blue (450 nm) μ -ILEDs being lighted. (b) Detailed layer structure of the micro-needle. (top) The device includes first layer of platinum microelectrode ($20\ \mu\text{m} \times 20\ \mu\text{m}$ exposed area) for recording and stimulating, second layer of Si μ -IPD ($1.25\text{-}\mu\text{m}$ thick, $200 \times 200\ \mu\text{m}^2$), third layer of 4 μ -ILEDs connected in parallel, and fourth layer of micro Pt temperature sensor or heater. (bottom) The side view of the device illustrates the ultrathin feature of the device. (c) (left) Soft optoelectronic wireless systems for optogenetics, including the energy harvester units and LEDs. Schematic illustration of implantation locations for the device on the peripheral nerves (middle) and the epidural space (right). (d) Sciatic stimulation to manipulate nociceptive responses. (top) Nociceptive pathways and LED stimulation. (bottom) Modified Y-maze, with one arm installed with the RF antenna to activate the LED stimulation (LED ON) and the other is not (LED OFF). (e) Heat maps representing the time a mice spent in each zone, with red indicating more time and blue indicating less time. With sciatic stimulation, aversion to the LED-ON zone is observed in TrpV1-ChR2 and Advillin-ChR2 mice. (With permission from McCall *et al.* 2013 [38], Nature Publishing Group.)(With permission from McCall *et al.* 2013 [38], Nature Publishing Group.)(With permission from Park *et al.* 2015 [39], Nature Publishing Group.)(With permission from Park *et al.* 2015 [39], Nature Publishing Group.)

ablation monitoring. Such ultrathin needle-type sensors can be inserted into the myocardial tissue in a minimally invasive manner to assist in the ablation process for treating arrhythmias [41].

10.4 Biodegradable Electronics

Implantable biosensors are another important category of biomedical devices to realize real-time monitoring of physiological signals inside the human body. Traditional biosensors are made in a bulk and hard format, and are designed to have a permanent lifetime. In some scenarios, implantable biosensors are only needed for a certain amount of time for monitoring purposes, such as tracking the post-surgery recovery of traumatic brain injury or identifying epileptic neural networks. Device removal is therefore necessary through a second surgery, without which there would be potential risks associated with inflammation and foreign body rejection. An ideal solution would be to build an implantable biosensor with all materials that can be safely absorbed by the body, a physically transient and disappearing biosensor, to avoid a second surgery. In order to build water-soluble and flexible devices, nanomembrane materials are desirable in order to achieve sensors with mechanical flexibility and limited amount of residual materials to be absorbed by the body.

Conventional biodegradable materials are mostly passive structural materials, such as biodegradable polymer materials for degradable sutures, cardiovascular stents, and scaffolds for tissue regeneration [42, 43]. In order to build high-performance functional systems, exploration for more biodegradable materials is necessary. Comprehensive investigations have been performed on inorganic materials that can dissolve in physiological environments. Dissolution measurements of metallic nanomembranes (40–300 nm) were performed by monitoring the resistance changes as a function of time on patterned serpentine metal traces in solutions with different pH and at different temperatures, with the dissolution rates defined as electrical dissolution rates (EDRs). It was found that metallic thin films, including magnesium (Mg), zinc (Zn), iron (Fe), molybdenum (Mo), and tungsten (W) all dissolve in simulated biofluids (Hanks' solutions) with different rates [44]. These nanomembrane conductors lose their electrical conductivity within a few hours for Mg and Zn and a few days to weeks for W and Mo, depending on the pH of the solutions, temperature, and deposition techniques. Dissolution proceeds in a nonuniform manner (e.g., pitting corrosion or formation of micropores) and complete material dissolution takes place afterwards in a longer timescale [44].

A simple 1D model of reactive diffusion that connects nanomembrane thickness directly to the resistance is capable of capturing the dissolution trends [45]. Resistance changes are represented by changes in an effective thickness (h) that accounts both for changes in physical thickness and for influences associated with porosity, pitting, and other nonuniformities. The model considers both chemical reactions and diffusion of water into the metal due to the formation of pores. The key parameters are the diffusivity of water in the metal film, D , and the reaction rate constant k . With $z = 0$ at the bottom surface of the metal, the

water concentration w at time t satisfies the reactive diffusion equation:

$$D\partial^2 w/\partial^2 z - kw = \partial w/\partial t \quad (10.1)$$

For a constant water concentration at the top surface of the metal $w|_{z=h_0} = w_0$ ($w_0 = 1 \text{ g cm}^{-3}$) and zero water flux $\partial w/\partial t|_{z=0} = 0$ at the bottom surface, the analytical solution to Eq. (10.1) can be obtained:

$$\frac{h}{h_0} \approx 1 - \frac{t}{t_c} \quad (10.2)$$

where h_0 is the initial thickness and $t_c = h_0 q \rho M_{\text{H}_2\text{O}} (\sqrt{kD} w_0 M)^{-1} \tanh^{-1} \sqrt{kh_0^2/D}$ is the critical time when the thickness reaches zero, ρ is the mass density of metal, and M and $M_{\text{H}_2\text{O}}$ are the molar masses of metal and water, respectively. The EDR can therefore be estimated according to

$$v_{\text{EDR}} = -\frac{dh}{dt} = \sqrt{kD} \frac{w_0 M}{q \rho M_{\text{H}_2\text{O}}} \tanh \sqrt{\frac{kh_0^2}{D}} \quad (10.3)$$

As the two free parameters D and k are not available in the literature data, they are acquired by fitting the model to the measured resistance curves.

Semiconductor nanomembranes (30–300 nm), such as single-crystal silicon (Si) [46], single-crystal germanium (Ge) [47], and amorphous indium–gallium–zinc oxide (a-IGZO) [48] are found to be dissolvable in physiological solutions with rates of a few nanometers per day. Dissolution rates are controlled by the pH values, ionic concentrations, and temperatures [49–51]. Density functional theory (DFT) and molecular dynamics (MD) simulation were performed to reveal the underlying physics of silicon dissolution behavior. The results suggest that silicon is susceptible to nucleophilic ions, and chlorides and phosphates above a certain level of concentration can significantly speed up silicon dissolution even in a near-neutral aqueous solution (pH 7.4) [50]. It is worth noting that the biodegradability of single-crystal silicon nanomembrane in biofluids enables fabricating degradable biosensors with high operational characteristics and allows the application of well-established Si technology to nonconventional biodegradable devices.

Moreover, dielectric materials, including magnesium oxide (MgO), silicon dioxide (SiO₂), spin-on-glass (SOG), and silicon nitride (Si₃N₄), are also dissolvable in biofluids [46, 52]. The dissolution rates are highly sensitive to the deposition methods which significantly influence the density of the thin films; for example, dissolution rates of oxides deposited through electron-beam (e-beam) evaporation is 100 times slower compared to that deposited through plasma-enhanced chemical vapor deposition (PECVD). Combining with biodegradable substrates, including silk, collagen, and US Food and Drug Administration (FDA)-approved biodegradable polymers (poly(lactic-co-glycolic acid) (PLGA), polycaprolactone, etc.) [46, 53], a fully dissolvable biosensor can be achieved.

As biodegradable materials are susceptible to solvents, heat, and water, new fabrication techniques are needed to avoid potential issues associated with traditional photolithography techniques. The single-crystal silicon nanomembrane

is transferred onto the target substrate as the active semiconductor component through the techniques described before [46]. The following deposition of metals and dielectric materials through a polyimide stencil mask was first developed to avoid possible damage to the biodegradable substrates through traditional photolithography techniques [46]. However, this process is limited by the resolution of the stencil mask, and new methods have been developed afterwards. Devices are fabricated on unusual SOI wafers with Si(111) as the substrate handle component, followed by silicon nitride encapsulation to protect the device underneath during the KOH undercut process to achieve transfer printing to biodegradable substrates [54]. Alternatively, the full device can be fabricated on an intermediate substrate followed by a second transfer printing process to the final substrates. As shown in Figure 10.3a, silicon nanomembranes from (001) SOI wafers are transfer printed on to an intermediate substrate (e.g., silicon/poly(methyl methacrylate)/diluted-polyimide (Si/PMMA/D-PI)) followed by the deposition of dielectric and metallic nanomembranes to achieve a full device. After spin-coating of a final supporting D-PI layer, the full device was picked up by PDMS stamp through an undercut process in solvent to remove the sacrificial PMMA layer. Following the removal of the bottom D-PI support, the device is transferred to the targeted biodegradable substrates along with etching of the top D-PI layer [53].

Extensive investigation of biocompatibility of the aforementioned materials has also been performed. Immune cells cultured on Si, Ge, SiGe, polycrystalline silicon (p-Si), amorphous silicon (a-Si), and SOG nanomembranes showed no cytotoxicity during the course of material degradation compared to negative control samples using high-density polyethylene (HDPE), indicating good biocompatibility of the degradation products [47, 51, 56]. Simple devices (silk, Mg on silk, MgO on silk, and Si on silk) were implanted in the subdermal region of mice models to assess the long-term tissue and immunologic biocompatibility. Immunoprofiling of lymphocytes and serum levels of proinflammatory cytokine studies show no significant difference compared to the control sample, indicating the tested devices are nonimmunogenic and biocompatible [49]. Implantation of an intracranial pressure (ICP) platform composed of Mo, porous silicon, doped Si, SiO₂, polyanhydride, and PLGA materials shows no inflammatory response over an observation window of 8 weeks [55]. In all, combining studies of a variety of dissolvable materials and development of novel fabrication techniques, various functional biosensors have become possible.

Arrays of dissolvable basic building blocks for integrated circuits were built, such as resistors, inductors, capacitors, diodes, and transistors [46]. Degradable thermal therapy systems were made by Mg wires and Si resistors on silk substrates [46]. Zinc oxide (ZnO) was adopted to construct a dissolvable piezoelectric energy harvester [57]. Wireless RF circuits were fabricated on silk substrates to enable remote communication for biosensors [58]. Fully degradable battery systems were developed on the basis of Mg and Mo metals with polyanhydride as the casing material [59]. Implantable drug delivery systems with programmable release have also been demonstrated using silk or lipid vehicles, and a controlled amount of drug can be delivered upon heat triggering [60, 61]. A resorbable electronic stent was fabricated on an Mg stent, integrating multifunctional

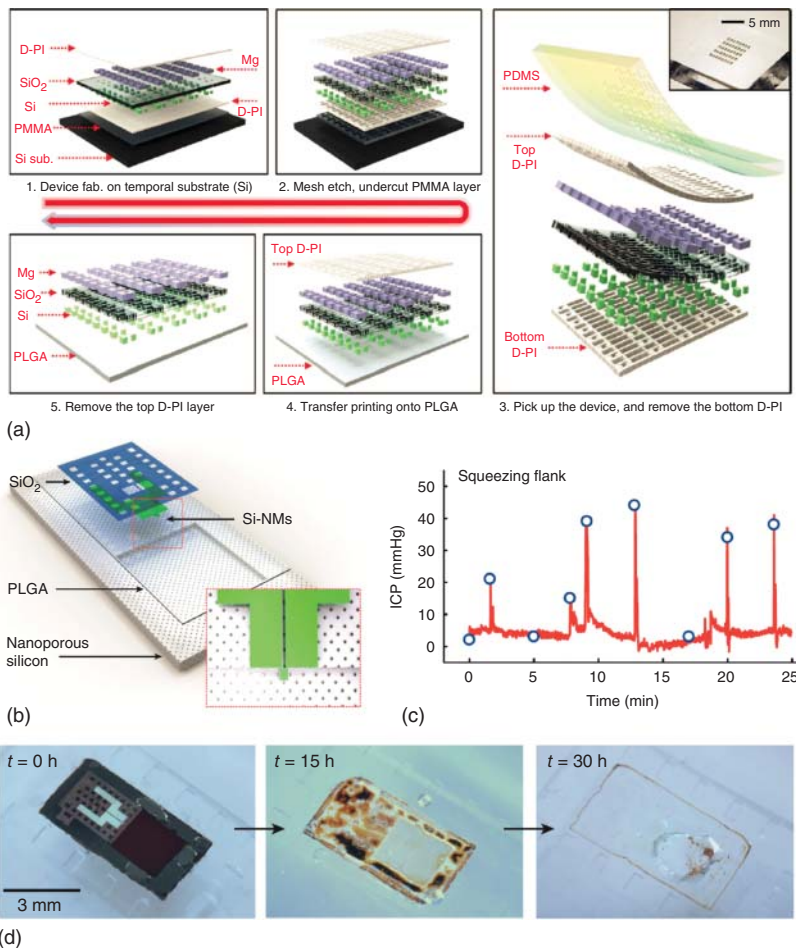


Figure 10.3 *Biodegradable electronics.* (a) Transfer printing process for biodegradable electronics. Si nanomembrane is first transfer printed onto Si/PMMA/D-PI substrate, followed by patterned deposition of dielectric and metallic materials. A top D-PI layer is deposited as a supporting layer for transfer printing. Both the top and the bottom D-PI layers are patterned into a mesh structure, and the device is released through PMMA undercut in acetone. PDMS stamp is used to pick up the device, followed by the etching of the bottom D-PI layer. The device is then retrieved on the PLGA substrate followed by a final etching of the top D-PI layer. (b) Schematic illustration of the biodegradable intracranial pressure (ICP) sensor. A trench is created on porous Si substrate covered by a PLGA layer. Serpentine doped Si resistor is fabricated on the edge of the trench and can respond to changes in pressure in the sense that the induced strain will feed back a change in resistance. The Si resistor is encapsulated by a layer of SiO₂ layer to prevent fast degradation. (c) The real-time wireless measurements of intracranial pressure by the bioreabsorbable sensor (red) demonstrate comparable results compared to that measured by a commercial sensor (blue). (d) Optical images collected at different stages of the accelerated dissolution of an ICP device in a transparent PDMS chamber (pH 12 buffer solution at room temperature). (With permission from Hwang *et al.* 2014 [53], John Wiley and Sons.)(With permission from Kang *et al.* 2016 [55], Nature Publishing Group.)(With permission from Kang *et al.* 2016 [55], Nature Publishing Group.)(With permission from Kang *et al.* 2016 [55], Nature Publishing Group.)

components including flow and temperature sensor, drug-infused functionalized NPs, data storage, wireless power and data transmission, hyperthermia therapy, and so on [62]. Two biodegradable diagnostic systems for the brain have been achieved lately, and have demonstrated their usage in animal models with great performance. One is the ICP and intracranial temperature (ICT) sensor fabricated on a porous silicon substrate, as shown in Figure 10.3b [55]. The air cavity is created on the porous silicon substrate (60–80 μm) by etching onto its surface with depth of 30–40 μm , and is covered and sealed by a PLGA membrane layer ($\sim 30 \mu\text{m}$). The PLGA membrane will deflect in response to brain pressure and the signal can be captured by a Si nanomembrane serpentine resistor fabricated on top of the PLGA layer next to the edge of the cavity through a piezoresistive mechanism. The Si electrode is covered by an SiO_2 encapsulation layer (100 nm) to work against fast degradation by the biofluids. The pressure and temperature measurements in the mice animal models show results comparable with those of the commercial nondegradable devices. As shown in Figure 10.3c, the wireless ICP measurements (red) reveal identical features compared to those of the commercial sensor (blue) as the periodic Valsalva maneuver was activated by manually compressing the rat's abdomen which produces a change in the ICP. The whole device is fully degradable in accelerated test within 30 h in a buffered solution (pH 12) at room temperature, as shown in Figure 10.3d. The other demonstrated brain biosensor is the biodegradable ECoG neural sensor. Both passive and active electrode arrays were achieved with multiplexing capability for spatiotemporal mapping of electrical activity from the cerebral cortex [63]. Highly doped silicon nanomembrane is used as the electrode due to its slow degradation rates as well as good electrical conductivity. Active neural electrode array is realized using Si as the active semiconductor component, Mo as the interconnects, and $\text{SiO}_2/\text{Si}_3\text{N}_4/\text{SiO}_2$ materials as inter-layer dielectrics (ILD) and encapsulation layer because of the good water permeation resistance. Such a biodegradable sensor platform can record spatially resolved epileptic activity in both acute and chronic fashion, and meanwhile reduces tissue reactivity compared to conventional ECoG electrodes.

10.5 Conclusions

This chapter summarizes advanced technologies integrating hard inorganic materials and soft organic materials in nanomembrane format that enable many opportunities in biomedical applications in both research and clinical domains. The development of nonconventional fabrication techniques and novel design of materials allow ultrathin biosensors that can either be conformally attached to soft tissues or organs in a minimally invasive fashion or can be implanted into the body and be safely absorbed after usage. Further research efforts will focus on discovery and expansion of more material options, and development of cost-effective manufacturing approaches that permit mass production of the devices. Other areas include further improvement of wireless communication systems, implantable energy harvesters, and encapsulation strategies that allow robust long-term implants. These directions in this emerging field can

be pursued in parallel to accelerate translating these technologies for clinical diagnostic and therapeutic practice relevant to improvements in human health.

References

- 1 Liu, J. and Wang, N. (2014) *Biosensors Based on Nanomaterials and Nanodevices*, Taylor & Francis Group, LLC, Boca Raton, FL.
- 2 Li, S., Singh, J., Li, H., and Banerjee, I.A. (2011) *Biosensor Nanomaterials*, Wiley-VCH Verlag & Co., Weinheim, Germany.
- 3 Campbell, P.K., Jones, K.E., Huber, R.J., Horch, K.W., and Normann, R.A. (1991) *IEEE Trans. Biomed. Eng.*, **38**, 758.
- 4 Nichols, S.P., Koh, A., Storm, W.L., Shin, J.H., and Schoenfish, M.H. (2013) *Chem. Rev.*, **113**, 2528.
- 5 Rogers, J.A. (2015) *JAMA*, **313**, 561.
- 6 Rogers, J.A., Lagally, M.G., and Nuzzo, R.G. (2011) *Nature*, **477**, 45.
- 7 Kim, D.-H., Ghaffari, R., Lu, N., and Rogers, J.A. (2012) *Annu. Rev. Biomed. Eng.*, **14**, 113.
- 8 Meitl, M.A., Zhu, Z.-T., Kumar, V., Lee, K.J., Feng, X., Huang, Y.Y., Adesida, I., Nuzzo, R.G., and Rogers, J.A. (2006) *Nat. Mater.*, **5**, 33.
- 9 Kim, D.-H., Viventi, J., Amsden, J.J., Xiao, J., Vigeland, L., Kim, Y.-S., Blanco, J.A., Panilaitis, B., Frechette, E.S., Contreras, D., Kaplan, D.L., Omenetto, F.G., Huang, Y., Hwang, K.-C., Zakin, M.R., Litt, B., and Rogers, J.A. (2010) *Nat. Mater.*, **9**, 511.
- 10 Kim, D.-H., Lu, N., Ghaffari, R., Kim, Y.-S., Lee, S.P., Xu, L., Wu, J., Kim, R.-H., Song, J., Liu, Z., Viventi, J., de Graff, B., Elolampi, B., Mansour, M., Slepian, M.J., Hwang, S., Moss, J.D., Won, S.-M., Huang, Y., Litt, B., and Rogers, J.A. (2011) *Nat. Mater.*, **10**, 316.
- 11 Webb, R.C., Bonifas, A.P., Behnaz, A., Zhang, Y., Yu, K.J., Cheng, H., Shi, M., Bian, Z., Liu, Z., Kim, Y.-S., Yeo, W.-H., Park, J.S., Song, J., Li, Y., Huang, Y., Gorbach, A.M., and Rogers, J.A. (2013) *Nat. Mater.*, **12**, 938.
- 12 Khang, D.-Y., Jiang, H., Huang, Y., and Rogers, J.A. (2006) *Science*, **311**, 208.
- 13 Fan, J.A., Yeo, W.-H., Su, Y., Hattori, Y., Lee, W., Jung, S.-Y., Zhang, Y., Liu, Z., Cheng, H., Falgout, L., Bajema, M., Coleman, T., Gregoire, D., Larsen, R.J., Huang, Y., and Rogers, J.A. (2014) *Nat. Commun.*, **5**.
- 14 Kim, D.-H., Lu, N., Ma, R., Kim, Y.-S., Kim, R.-H., Wang, S., Wu, J., Won, S.M., Tao, H., Islam, A., Yu, K.J., Kim, T.-i., Chowdhury, R., Ying, M., Xu, L., Li, M., Chung, H.-J., Keum, H., McCormick, M., Liu, P., Zhang, Y.-W., Omenetto, F.G., Huang, Y., Coleman, T., and Rogers, J.A. (2011) *Science*, **333**, 838.
- 15 Kim, D.H., Ahn, J.H., Kim, H.S., Lee, K.J., Kim, T.H., Yu, C.J., Nuzzo, R.G., and Rogers, J.A. (2008) *IEEE Electron Device Lett.*, **29**, 73.
- 16 Ahn, J.-H., Kim, H.-S., Lee, K.J., Zhu, Z., Menard, E., Nuzzo, R.G., and Rogers, J.A. (2006) *IEEE Electron Device Lett.*, **27**, 460.
- 17 Ahn, J.-H., Kim, H.-S., Menard, E., Lee, K.J., Zhu, Z., Kim, D.-H., Nuzzo, R.G., and Rogers, J.A. (2007) *Appl. Phys. Lett.*, **90**, p. 213501.

- 18 Kim, D.-H., Ahn, J.-H., Choi, W.M., Kim, H.-S., Kim, T.-H., Song, J., Huang, Y.Y., Liu, Z., Lu, C., and Rogers, J.A. (2008) *Science*, **320**, 507.
- 19 Yoon, J., Baca, A.J., Park, S.-I., Elvikis, P., Geddes, J.B., Li, L., Kim, R.H., Xiao, J., Wang, S., Kim, T.-H., Motala, M.J., Ahn, B.Y., Duoss, E.B., Lewis, J.A., Nuzzo, R.G., Ferreira, P.M., Huang, Y., Rockett, A., and Rogers, J.A. (2008) *Nat. Mater.*, **7**, 907.
- 20 Ko, H.C., Stoykovich, M.P., Song, J., Malyarchuk, V., Choi, W.M., Yu, C.-J., Geddes, J.B., Xiao, J., Wang, S., Huang, Y., and Rogers, J.A. (2008) *Nature*, **454**, 748.
- 21 Song, Y.M., Xie, Y., Malyarchuk, V., Xiao, J., Jung, I., Choi, K.-J., Liu, Z., Park, H., Lu, C., Kim, R.-H., Li, R., Crozier, K.B., Huang, Y., and Rogers, J.A. (2013) *Nature*, **497**, 95.
- 22 Park, S.-I., Xiong, Y., Kim, R.-H., Elvikis, P., Meitl, M., Kim, D.-H., Wu, J., Yoon, J., Yu, C.-J., Liu, Z., Huang, Y., Hwang, K.-c., Ferreira, P., Li, X., Choquette, K., and Rogers, J.A. (2009) *Science*, **325**, 977.
- 23 Kim, R.-H., Kim, D.-H., Xiao, J., Kim, B.H., Park, S.-I., Panilaitis, B., Ghaffari, R., Yao, J., Li, M., Liu, Z., Malyarchuk, V., Kim, D.G., Le, A.-P., Nuzzo, R.G., Kaplan, D.L., Omenetto, F.G., Huang, Y., Kang, Z., and Rogers, J.A. (2010) *Nat. Mater.*, **9**, 929.
- 24 Viventi, J., Kim, D.-H., Vigeland, L., Frechette, E.S., Blanco, J.A., Kim, Y.-S., Avrin, A.E., Tiruvadi, V.R., Hwang, S.-W., Vanleer, A.C., Wulsin, D.F., Davis, K., Gelber, C.E., Palmer, L., Van der Spiegel, J., Wu, J., Xiao, J., Huang, Y., Contreras, D., Rogers, J.A., and Litt, B. (2011) *Nat. Neurosci.*, **14**, 1599.
- 25 Viventi, J., Kim, D.-H., Moss, J.D., Kim, Y.-S., Blanco, J.A., Annetta, N., Hicks, A., Xiao, J., Huang, Y., Callans, D.J., Rogers, J.A., and Litt, B. (2010) *Sci. Transl. Med.*, **2**, 24ra22.
- 26 Xu, L., Gutbrod, S.R., Bonifas, A.P., Su, Y., Sulkin, M.S., Lu, N., Chung, H.-J., Jang, K.-I., Liu, Z., Ying, M., Lu, C., Webb, R.C., Kim, J.-S., Laughner, J.I., Cheng, H., Liu, Y., Ameen, A., Jeong, J.-W., Kim, G.-T., Huang, Y., Efimov, I.R., and Rogers, J.A. (2014) *Nat. Commun.*, **5**.
- 27 Huang, X., Yeo, W.-H., Liu, Y., and Rogers, J.A. (2012) *Biointerphases*, **7**, 52.
- 28 Huang, X., Cheng, H., Chen, K., Zhang, Y., Zhang, Y., Liu, Y., Zhu, C., Ouyang, S.-c., Kong, G.-W., Yu, C., Huang, Y., and Rogers, J.A. (2013) *IEEE Trans. Biomed. Eng.*, **60**, 2848.
- 29 Huang, X., Liu, Y., Chen, K., Shin, W.-J., Lu, C.-J., Kong, G.-W., Patnaik, D., Lee, S.-H., Cortes, J.F., and Rogers, J.A. (2014) *Small*, **10**, 3083.
- 30 Ying, M., Bonifas, A.P., Lu, N., Su, Y., Li, R., Cheng, H., Ameen, A., Huang, Y., and Rogers, J.A. (2012) *Nanotechnology*, **23**, p. 344004.
- 31 Jeong, J.-W., Yeo, W.-H., Akhtar, A., Norton, J.J.S., Kwack, Y.-J., Li, S., Jung, S.-Y., Su, Y., Lee, W., Xia, J., Cheng, H., Huang, Y., Choi, W.-S., Bretl, T., and Rogers, J.A. (2013) *Adv. Mater.*, **25**, 6839.
- 32 Hattori, Y., Falgout, L., Lee, W., Jung, S.-Y., Poon, E., Lee, J.W., Na, I., Geisler, A., Sadhwani, D., Zhang, Y., Su, Y., Wang, X., Liu, Z., Xia, J., Cheng, H., Webb, R.C., Bonifas, A.P., Won, P., Jeong, J.-W., Jang, K.-I., Song, Y.M., Nardone, B., Nodzenski, M., Fan, J.A., Huang, Y., West, D.P., Paller, A.S., Alam, M., Yeo, W.-H., and Rogers, J.A. (2014) *Adv. Healthc. Mater.*, **3**, 1597.

- 33 Dagdeviren, C., Su, Y., Joe, P., Yona, R., Liu, Y., Kim, Y.-S., Huang, Y., Damadoran, A.R., Xia, J., Martin, L.W., Huang, Y., and Rogers, J.A. (2014) *Nat. Commun.*, **5**.
- 34 Dagdeviren, C., Shi, Y., Joe, P., Ghaffari, R., Balooch, G., Usgaonkar, K., Gur, O., Tran, P.L., Crosby, J.R., Meyer, M., Su, Y., Chad Webb, R., Tedesco, A.S., Slepian, M.J., Huang, Y., and Rogers, J.A. (2015) *Nat. Mater.*, **14**, 728.
- 35 Norton, J.J.S., Lee, D.S., Lee, J.W., Lee, W., Kwon, O., Won, P., Jung, S.-Y., Cheng, H., Jeong, J.-W., Akce, A., Umunna, S., Na, I., Kwon, Y.H., Wang, X.-Q., Liu, Z., Paik, U., Huang, Y., Bretl, T., Yeo, W.-H., and Rogers, J.A. (2015) *Proc. Natl. Acad. Sci. U.S.A.*, **112**, 3920.
- 36 Huang, X., Liu, Y., Cheng, H., Shin, W.-J., Fan, J.A., Liu, Z., Lu, C.-J., Kong, G.-W., Chen, K., Patnaik, D., Lee, S.-H., Hage-Ali, S., Huang, Y., and Rogers, J.A. (2014) *Adv. Funct. Mater.*, **24**, 3846.
- 37 Kim, T.-i., McCall, J.G., Jung, Y.H., Huang, X., Siuda, E.R., Li, Y., Song, J., Song, Y.M., Pao, H.A., Kim, R.-H., Lu, C., Lee, S.D., Song, I.-S., Shin, G., Al-Hasani, R., Kim, S., Tan, M.P., Huang, Y., Omenetto, F.G., Rogers, J.A., and Bruchas, M.R. (2013) *Science*, **340**, 211.
- 38 McCall, J.G., Kim, T.-i., Shin, G., Huang, X., Jung, Y.H., Al-Hasani, R., Omenetto, F.G., Bruchas, M.R., and Rogers, J.A. (2013) *Nat. Protoc.*, **8**, 2413.
- 39 Park, S.I., Brenner, D.S., Shin, G., Morgan, C.D., Copits, B.A., Chung, H.U., Pullen, M.Y., Noh, K.N., Davidson, S., Oh, S.J., Yoon, J., Jang, K.-I., Samineni, V.K., Norman, M., Grajales-Reyes, J.G., Vogt, S.K., Sundaram, S.S., Wilson, K.M., Ha, J.S., Xu, R., Pan, T., Kim, T.-i., Huang, Y., Montana, M.C., Golden, J.P., Bruchas, M.R., Gereau Iv, R.W., and Rogers, J.A. (2015) *Nat. Biotechnol.*, **33**, 1280.
- 40 J.-W. Jeong, Jordan G. McCall, G. Shin, Y. Zhang, R. Al-Hasani, M. Kim, S. Li, J. Y. Sim, K.-I. Jang, Y. Shi, Daniel Y. Hong, Y. Liu, Gavin P. Schmitz, L. Xia, Z. He, P. Gamble, Wilson Z. Ray, Y. Huang, Michael R. Bruchas, John A. Rogers, (2015) *Cell* **162**, 662.
- 41 Koh, A., Gutbrod, S.R., Meyers, J.D., Lu, C., Webb, R.C., Shin, G., Li, Y., Kang, S.-K., Huang, Y., Efimov, I.R., and Rogers, J.A. (2016) *Adv. Healthc. Mater.*, **5**, 373.
- 42 Freed, L.E., Vunjak-Novakovic, G., Biron, R.J., Eagles, D.B., Lesnoy, D.C., Barlow, S.K., and Langer, R. (1994) *Nat. Biotechnol.*, **12**, 689.
- 43 Stone, G.W., Ellis, S.G., Cox, D.A., Hermiller, J., O'Shaughnessy, C., Mann, J.T., Turco, M., Caputo, R., Bergin, P., Greenberg, J., Popma, J.J., and Russell, M.E. (2004) *New Engl. J. Med.*, **350**, 221.
- 44 Yin, L., Cheng, H., Mao, S., Haasch, R., Liu, Y., Xie, X., Hwang, S.-W., Jain, H., Kang, S.-K., Su, Y., Li, R., Huang, Y., and Rogers, J.A. (2014) *Adv. Funct. Mater.*, **24**, 645.
- 45 Li, R., Cheng, H., Su, Y., Hwang, S.-W., Yin, L., Tao, H., Brenckle, M.A., Kim, D.-H., Omenetto, F.G., Rogers, J.A., and Huang, Y. (2013) *Adv. Funct. Mater.*, **23**, 3106–3114.
- 46 Hwang, S.-W., Tao, H., Kim, D.-H., Cheng, H., Song, J.-K., Rill, E., Brenckle, M.A., Panilaitis, B., Won, S.M., Kim, Y.-S., Song, Y.M., Yu, K.J., Ameen, A., Li, R., Su, Y., Yang, M., Kaplan, D.L., Zakin, M.R., Slepian, M.J., Huang, Y., Omenetto, F.G., and Rogers, J.A. (2012) *Science*, **337**, 1640.

- 47 Kang, S.-K., Park, G., Kim, K., Hwang, S.-W., Cheng, H., Shin, J., Chung, S., Kim, M., Yin, L., Lee, J.C., Lee, K.-M., and Rogers, J.A. (2015) *ACS Appl. Mater. Interfaces*, **7**, 9297.
- 48 Jin, S.H., Kang, S.-K., Cho, I.-T., Han, S.Y., Chung, H.U., Lee, D.J., Shin, J., Baik, G.W., Kim, T.-i., Lee, J.-H., and Rogers, J.A. (2015) *ACS Appl. Mater. Interfaces*, **7**, 8268.
- 49 Hwang, S.-W., Park, G., Cheng, H., Song, J.-K., Kang, S.-K., Yin, L., Kim, J.-H., Omenetto, F.G., Huang, Y., Lee, K.-M., and Rogers, J.A. (2014) *Adv. Mater.*, **26**, 1992.
- 50 Yin, L., Farimani, A.B., Min, K., Vishal, N., Lam, J., Lee, Y.K., Aluru, N.R., and Rogers, J.A. (2015) *Adv. Mater.*, **27**, 1857.
- 51 Hwang, S.-W., Park, G., Edwards, C., Corbin, E.A., Kang, S.-K., Cheng, H., Song, J.-K., Kim, J.-H., Yu, S., Ng, J., Lee, J.E., Kim, J., Yee, C., Bhaduri, B., Su, Y., Omenetto, F.G., Huang, Y., Bashir, R., Goddard, L., Popescu, G., Lee, K.-M., and Rogers, J.A. (2014) *ACS Nano*, **8**, 5843.
- 52 Kang, S.-K., Hwang, S.-W., Cheng, H., Yu, S., Kim, B.H., Kim, J.-H., Huang, Y., and Rogers, J.A. (2014) *Adv. Funct. Mater.*, **24**, 4427.
- 53 Hwang, S.-W., Song, J.-K., Huang, X., Cheng, H., Kang, S.-K., Kim, B.H., Kim, J.-H., Yu, S., Huang, Y., and Rogers, J.A. (2014) *Adv. Mater.*, **26**, 3905.
- 54 Hwang, S.-W., Kim, D.-H., Tao, H., Kim, T.-i., Kim, S., Yu, K.J., Panilaitis, B., Jeong, J.-W., Song, J.-K., Omenetto, F.G., and Rogers, J.A. (2013) *Adv. Funct. Mater.*, **23**, 4087.
- 55 Kang, S.-K., Murphy, R.K.J., Hwang, S.-W., Lee, S.M., Harburg, D.V., Krueger, N.A., Shin, J., Gamble, P., Cheng, H., Yu, S., Liu, Z., McCall, J.G., Stephen, M., Ying, H., Kim, J., Park, G., Webb, R.C., Lee, C.H., Chung, S., Wie, D.S., Gujar, A.D., Vemulapalli, B., Kim, A.H., Lee, K.-M., Cheng, J., Huang, Y., Lee, S.H., Braun, P.V., Ray, W.Z., and Rogers, J.A. (2016) *Nature*, **530**, 71.
- 56 Kang, S.-K., Hwang, S.-W., Yu, S., Seo, J.-H., Corbin, E.A., Shin, J., Wie, D.S., Bashir, R., Ma, Z., and Rogers, J.A. (2015) *Adv. Funct. Mater.*, **25**, 1789.
- 57 Dagdeviren, C., Hwang, S.-W., Su, Y., Kim, S., Cheng, H., Gur, O., Haney, R., Omenetto, F.G., Huang, Y., and Rogers, J.A. (2013) *Small*, **9**, 3398.
- 58 Hwang, S.-W., Huang, X., Seo, J.-H., Song, J.-K., Kim, S., Hage-Ali, S., Chung, H.-J., Tao, H., Omenetto, F.G., Ma, Z., and Rogers, J.A. (2013) *Adv. Mater.*, **25**, 3526.
- 59 Yin, L., Huang, X., Xu, H., Zhang, Y., Lam, J., Cheng, J., and Rogers, J.A. (2014) *Adv. Mater.*, **26**, 3879.
- 60 Tao, H., Hwang, S.-W., Marelli, B., An, B., Moreau, J.E., Yang, M., Brenckle, M.A., Kim, S., Kaplan, D.L., Rogers, J.A., and Omenetto, F.G. (2014) *Proc. Natl. Acad. Sci. U.S.A.*, **111**, 17385.
- 61 Lee, C.H., Kim, H., Harburg, D.V., Park, G., Ma, Y., Pan, T., Kim, J.S., Lee, N.Y., Kim, B.H., Jang, K.-I., Kang, S.-K., Huang, Y., Kim, J., Lee, K.-M., Leal, C., and Rogers, J.A. (2015) *NPG Asia Mater.*, **7**, e227.
- 62 Son, D., Lee, J., Lee, D.J., Ghaffari, R., Yun, S., Kim, S.J., Lee, J.E., Cho, H.R., Yoon, S., Yang, S., Lee, S., Qiao, S., Ling, D., Shin, S., Song, J.-K., Kim, J., Kim, T., Lee, H., Kim, J., Soh, M., Lee, N., Hwang, C.S., Nam, S., Lu, N., Hyeon, T., Choi, S.H., and Kim, D.-H. (2015) *ACS Nano*, **9**, 5937.

- 63 Yu, K.J., Kuzum, D., Hwang, S.-W., Kim, B.H., Juul, H., Kim, N.H., Won, S.M., Chiang, K., Trumpis, M., Richardson, A.G., Cheng, H., Fang, H., Thompson, M., Bink, H., Talos, D., Seo, K.J., Lee, H.N., Kang, S.-K., Kim, J.-H., Lee, J.Y., Huang, Y., Jensen, F.E., Dichter, M.A., Lucas, T.H., Viventi, J., Litt, B., and Rogers, J.A. (2016) *Nat. Mater.*, **15**, pp. 782–791.